J. Fluid Mech. (2007), *vol.* 581, *pp.* 371–399.
doi:10.1017/S002211200700568X Printed in the United Kingdom

Shipping of water on a two-dimensional structure. Part 2

M. GRECO[1,2], G. COLICCHIO[1,2] AND O. M. FALTINSEN[2]

[1]INSEAN, The Italian Ship Model Basin, Via di Vallerano 139, 00128 Roma, Italy
[2]Centre for Ships and Ocean Structures (CESOS), NTNU, Norway

(Received 18 October 2005 and in revised form 4 January 2007)

The water-shipping problem is modelled in a two-dimensional framework and studied experimentally and numerically for the case of a fixed barge-shaped structure. The analysis represents the second step of the research discussed in Greco *et al.* (*J. Fluid Mech.*, vol. 525, 2005, p. 309). The numerical investigation is performed by using both a boundary element method and a domain-decomposition strategy. The model tests highlight the occurrence of dam-breaking-type water on deck, (*a*) with and (*b*) without an initial plunging phase, and (*c*) an unusual type of water shipping connected with blunt water–deck impacts here called a hammer-fist type event never documented before. Cases (*a*) and (*c*) are connected with the most severe events and the related features and green-water loads are discussed in detail. A parametric analysis of water-on-deck phenomena has also been carried out in terms of the local incoming waves and bow flow features. We classify such phenomena in a systematic way to provide a basis for further investigations of water-on-deck events. The severity of (*a*)-type water-on-deck events is analysed in terms of initial cavity area and water-front velocity along the deck. The former increases as the square power of the modified incoming-wave (front-crest) steepness while the latter scales with its square-root. The two-dimensional investigation gives useful quantitative information in terms of water-front velocity for comparison with three-dimensional water-on-deck experiments on fixed bow models interacting with wave packets.

1. Introduction

Compact masses of water (green water) shipped onto the deck of vessels represent a danger for the dynamic ship stability and the structural stability because of the resulting loads on the deck, superstructures and equipment. The consequences can vary depending on the vessel type, the operational conditions, and the sea state causing the water-on-deck event.

In terms of the global features, two main water-on-deck scenarios have been identified: one (DB) where the flow of water onto the deck resembles that following the breaking of a dam and one (PW) where the water is shipped as a large-scale plunging breaker hitting the deck or the superstructures (cf. MARINTEK 2000; Faltinsen 2005). Type PW is less common and occurs in connection with steep, almost breaking, waves interacting with the ship. It is potentially more dangerous for the vessel due to its kinematic and dynamic features and the larger amount of water usually associated with it. Usually the water-on-deck phenomena have features common to both scenarios.

A two-dimensional investigation of the water shipping phenomenon is presented in Greco, Landrini & Faltinsen (2005) for a fixed barge-shaped structure. The analysis is relevant for 'Floating Production Storage and Offloading' (FPSO) types of oil platforms and in general for vessels without forward motion. The problem was studied both experimentally and numerically through a boundary element method (BEM) for unsteady nonlinear free-surface flows.

Two tools were used to investigate the water on deck in terms of both the flow evolution and the pressures induced on a vertical superstructure placed on the deck. For most of the cases studied, the water shipping observed experimentally was characterized by an initial plunging phase at the bow leading to an impact with the deck and air entrainment. This appeared as a localized phenomenon both in space and time. The later stages showed a DB type behaviour. The BEM was able to describe the main features of the water shipping but required the explicit enforcement of a deck-edge condition (see § 3.3 in Greco *et al.* 2005) and then two separate simulations of the water shipping to describe the initial plunging and the further DB-type evolution, respectively. Moreover, it is not able to capture the later stages which involve free-surface breaking and fragmentation, air entrainment, and possible viscous effects.

The analysis of such phenomena required the use of a more general numerical tool, not based on the potential flow assumption, and combined with a suitable technique to follow the air–water interface beyond the occurrence of breaking. In this context, much effort has been made by the numerical community to develop effective and robust tools. A two-dimensional study of the flow evolution and green-water loads is presented by Nielsen & Mayer (2004) combining a single-phase (water) Navier–Stokes solver with a volume-of-fluid (VOF) technique for the free-surface evolution.

Three-dimensional experimental–numerical studies are reported in Kleefsman *et al.* (2002) and Wemmenhove *et al.* (2005) in the case of single-phase (water) and two-phase (water and air) flows, respectively. The former work documented only DB type of water on deck and modelled it numerically as an equivalent three-dimensional dam-breaking problem. This limited the challenges in terms of memory space and CPU-time because the wave-generation and wave-damping processes were not described numerically. In the latter work, a three-dimensional dam-breaking model test is carried out and used to validate the numerical tool. The impact on superstructures is also investigated. Three-dimensional water-on-deck simulations of green-water events using the CIP method are presented by Faltinsen, Zhu & Hu (2005) for a Wigley hull in forward motion. The flow evolution is analysed but no comparison with experiments is reported. From the results, the need of a finer discretization is evident but the numerical solution appears promising in describing qualitatively the flow phenomenon.

Here the generalization of the numerical tool is achieved within a domain-decomposition strategy (see Quarteroni & Valli 1999; Campana & Iafrati 2001) to keep the advantages offered by the BEM when applicable, namely its efficiency and accuracy in handling free-surface flows. In the zonal approach, the BEM is used in an outer region while a suitable field solver is adopted in an inner region containing the vessel where the water shipping and all related physical mechanisms occur. The method is validated and used in the physical analysis of the water-on-deck events discussed in Greco *et al.* (2005) and to investigate other unusual water shipping phenomena detected in the model tests and not analysed before.

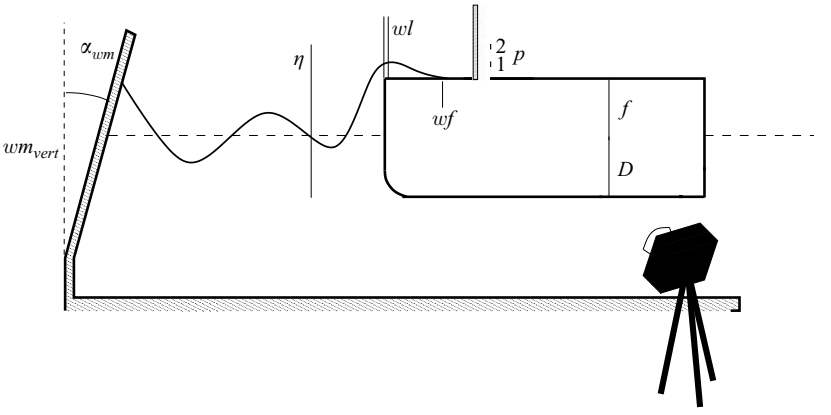

FIGURE 1. Water on deck at the bow of a two-dimensional stationary ship restrained from oscillating. Sketch of the experimental set-up, main parameters and sensors. Side view.

The present study is mostly relevant for stationary ships with blunt bow forms. It is not intended to be a comprehensive analysis of the body and incoming-wave parameters, but it examines the water-on-deck features in terms of some important incoming-wave and kinematic variables. A two-dimensional model is adopted, so the information is mostly qualitative. However, it contributes to a deeper understanding and classification of the water-shipping scenarios.

The experiments are briefly described in the next section, the numerical method is reported in § 3 and their combined studies are discussed in § 4. The main conclusions are drawn in § 5.

2. Model tests

Two-dimensional model tests were carried out in a narrow flume 13.5 m long, 1.035 m deep and 0.6 m wide at the Department of Marine Hydrodynamics, NTNU. The incoming waves were generated by a flap wavemaker and the water-on-deck events caused by their interaction with a fixed barge-shaped model were investigated. The body was in Plexiglas with draft $D = 0.198$ m, length $L = 1.5$ m and freeboard $f = 0.05$ m and placed at about 5.54 m from the wavemaker in its vertical position ($\mathrm{wm_{vert}}$).

The tests were performed both without and with a vertical wall along the deck, 0.2275 m from the bow edge. The sketch in figure 1 is a qualitative side view of the set-up and shows the variables examined here: the wavemaker time history recorded during the model tests in terms of evolution of the flap angle (α_{wm}); the wave elevation (η) measured 0.104 m from the bow by a cylindrical capacitive probe; the freeboard exceedance by the water at the bow (wl) measured by a non-intrusive capacitive probe; the water front propagation along the deck (wf) measured by a non-intrusive capacitive probe; the pressure evolution (p) recorded along the vertical superstructure 12 and 32 mm from the deck by piezoelectric pressure gauges ($p1$ and $p2$); the evolution of the shipped water along the deck captured by a low-speed camera with a frame rate of 25 frames per second.

The details of the experimental set-up can be found in Greco (2001) and Greco *et al.* (2005).

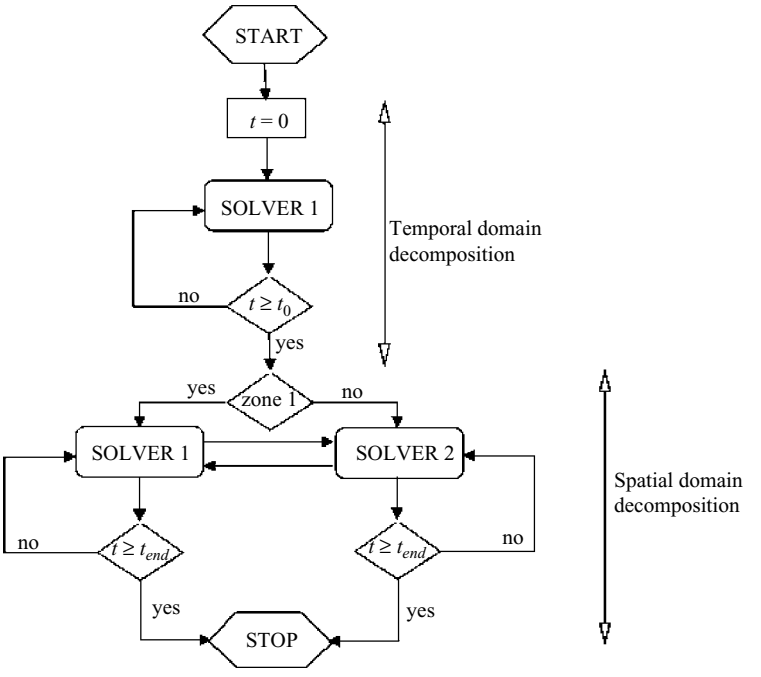

FIGURE 2. Flow diagram of the time–space domain-decomposition strategy with two solvers. SOLVER 1 = BEM. SOLVER 2 = NS solver.

3. Numerical method

In order to overcome the inability of the boundary element method (BEM) to analyse the whole picture of the water-on-deck phenomenon but to retain as far as possible its qualities of accuracy and efficiency (see Greco *et al.* 2005), a domain decomposition (DD) strategy has been developed where the potential-flow method is coupled with a field method. A Navier–Stokes (NS) solver has been preferred to an Euler solver because the minor increase in computational costs is balanced by the ability to handle the viscous flow-field effects possibly connected with free-surface breaking and air entrainment.

While viscosity may be important in the flow field, the comparisons in Greco *et al.* (2005) between the BEM results and green-water experiments confirmed a limited role of the boundary layer along the deck and the superstructure, both for the global evolution of the shipped water and its interaction with the vertical superstructure. Thus, here there is no attempt to handle the boundary layer of the body. This avoids the need of a very fine grid and limits the memory space and CPU-time requirements. Moreover, for efficient and simple modelling, the viscous flow is also assumed laminar, though this may not be the case and the possible influence of turbulence requires further study.

Within a zonal approach, the problem is solved by means of two (in principle many) solvers used to analyse different portions of the domain of interest. The splitting procedure can be either in time or in space or may involve both. Here the BEM and NS solvers are used within a time-space domain decomposition as shown in figure 2. In order to solve the water-on-deck problem in the most efficient and accurate way, the BEM is used to analyse the whole fluid domain for time t less than a threshold time instant t_0. At time $t = t_0$, when impact phenomena, large

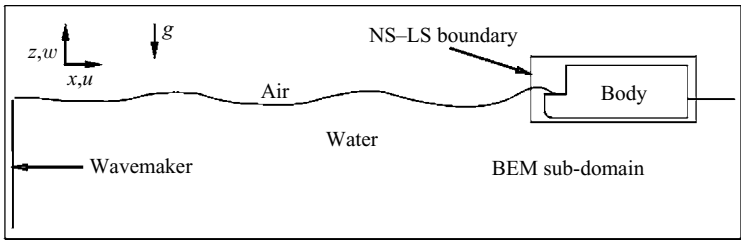

FIGURE 3. Domain-decomposition strategy applied to the water-on-deck problem. The incoming waves are generated on the left and interact with a ship-like structure. The damping region downstream of the body is not shown. The horizontal size of the NS–LS region (bounded by the solid box) is about 0.08 times the domain extent. For the simulations in § 4 $x = 0$ is at the centre of the ship model and $z = 0$ is at the undisturbed free surface.

deformations and fragmentation of the air–water interface (FS), air entrainment and pronounced viscous effects are likely to occur, the computational domain is split in two sub-domains: (i) an inner region containing the ship and solved through an NS solver combined with a level-set (LS) technique to capture properly the evolution of the air–water interface, and (o) an outer region surrounding it analysed through a BEM solver (see figure 3). The BEM solution at t_0 is used to initialize the field method solution.

In (i) the water-on-deck events will occur, in (o) incident waves are generated, propagate toward the vessel and damp out far downstream of the ship model. The damping (numerical wave beach) model is described by Greco (2001). In both sub-domains surface tension is neglected, and air and water flows are assumed incompressible even though the air should be considered compressible. The former approximation has been adopted because the scales of the most important phenomena are sufficiently large for the surface tension to play no significant role as shown in Greco *et al.* (2005). The latter approximation avoids the difficulties in the coupling of incompressible and compressible phases and limits the CPU-time requirements.

The zonal approach has been applied to two-dimensional cases, but no restrictions exist for extension to three-dimensional flows. Comprehensive descriptions of the BEM, the NS–LS solver and the DD strategy can be found in Greco (2001), Colicchio, Landrini & Chaplin (2005) and Colicchio, Greco & Faltinsen (2006), respectively.

3.1. *Boundary element method*

Here a two-dimensional air–water flow is considered, evolving in time according to the potential flow theory. The water is assumed unaffected by the air flow. This is a reasonable approximation as long as air cushions do not occur, and leads to a more efficient method. The air–water interface in this sub-domain is assumed to be a sharp surface across which the tangential velocity component is discontinuous.

Both liquid and gas problems are solved numerically in terms of the velocity potential φ by using the BEM described in Greco *et al.* (2005). This is combined with a second-order Runge–Kutta scheme for the time integration within the mixed Eulerian–Lagrangian approach. Once the problem in water has been solved, that in air is analysed by enforcing the continuity of the normal velocity across the air–water interface. The pressure is obtained from the Bernoulli equation. This requires the time derivative of the velocity potential φ_t, evaluated here similarly to φ. Once the problem in water has been solved, the continuity of the normal derivative of φ_t is enforced across the air–water interface and used as boundary condition for the problem in air.

3.2. *Navier–Stokes solver* plus *a level-set technique*

Here air and water are assumed coupled and in laminar isothermal conditions. Their evolutions are analysed by using a one-fluid formulation, that is the gas and liquid phases are modelled as a single fluid with properties (i.e. density, viscosity, etc.) continuously varying across an interface layer. In this way the conditions at the interface do not need to be explicitly enforced since they are implicitly fulfilled (see e.g. Wehausen & Laitone 1960) and the governing equations are formally identical to the continuity and Navier–Stokes equations for a single fluid. The resulting system of equations is solved on an Eulerian Cartesian fixed staggered grid through a finite-difference scheme coupled with a projection method using a second-order approximation both in space and time (see Colicchio *et al.* 2005 for details).

The location of the free surface is captured using a level-set (LS) function, ϕ, that represents the normal distance with sign, i.e. it is positive in air and negative in water, from the air–water interface (see e.g. Sethian 1999). A similar procedure is used to model the presence of an inner body, i.e. the body configuration is reconstructed once the normal distance with sign (positive/negative for points outside/inside the body), ψ, from its surface is known. Obtaining ϕ and ψ involves a numerical smoothing of the field variables across the air–water interface and the body surface, respectively. The geometrical properties of the body level-set function ψ are used to make ϕ symmetric with respect to the body surface. Consequently density and viscosity are initialized symmetrically in a thin layer inside the body.

A detailed description of the solution method can be found in Colicchio *et al.* (2005). The solver has been tested successfully on several simplified problems of interest in hydrodynamics, involving wave-breaking and air-entrapment phenomena and fluid–body interactions. Local and global convergence properties have been investigated in detail and numerical parameters were carefully chosen on the basis of these validation and convergence analyses.

3.3. *Domain-decomposition strategy*

The DD algorithm developed has been chosen in order to deal with cases where the air–water interface (*a*) intersects the transmission boundary and (*b*) can be highly deformed across such region. The strategy is based on an intrinsic coupling between overlapping sub-domains. The presence of an overlap means an increase in CPU time and memory space since both solvers analyse the problem there. However it leads to a more robust and stable code when conditions (*a*) and (*b*) are involved. Further, the discretizations of the communicating overlapping sub-domains are not forced to be very similar, since the information from one solver (donor) to the other (receiver) is transferred from inside the donor to the boundary of the receiver.

In a zonal approach, the crucial steps are the transmission of all the required information (domain-decomposition, DD, step) and its correction to make it consistent with the receiver solver (domain-composition, DC, step). In our case velocity, pressure and air–water interface data must be exchanged between the two solvers. In the BEM the data are needed at its transmission boundary and they must not be smoothed across the interface. The NS–LS also needs the information inside its sub-domain to make the boundary conditions smoothed consistently with the smoothing laws used around the free surface. The numerical features of the method are detailed and extensively discussed in Colicchio *et al.* (2006). The solver was validated against model tests and other numerical benchmark results. The sensitivity of the solution to the numerical parameters (i.e. the location and extent of the overlap region between the sub-domains, and effects of an improper DD–DC strategy) and the

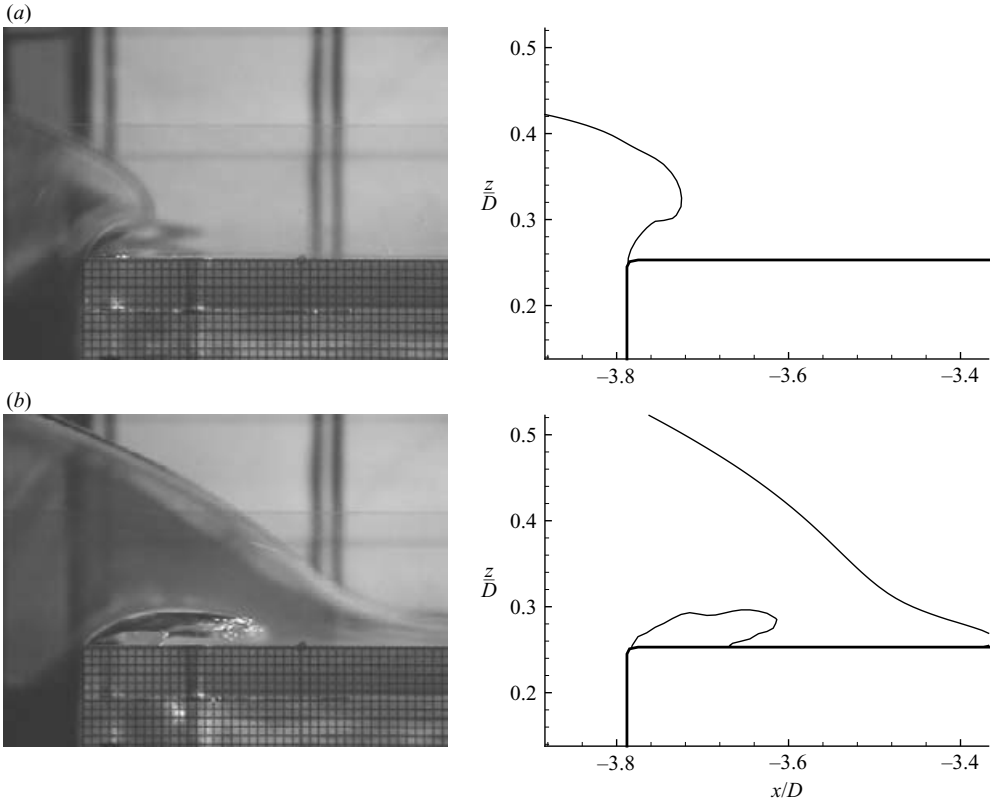

FIGURE 4. Initial plunging plus dam-breaking (PDB) type event: air-entrainment phenomenon. Left: experimental snapshots. Right: DD–DC air–water interface. Time increases from (*a*) to (*b*) with time interval of 0.12 s. Nominal incoming waves with $\lambda/f = 40$ and $H/\lambda = 0.08$.

convergence properties were also investigated. From that study, a good compromise between efficiency and robustness was obtained by using an overlap width of $10\Delta x$, with $\Delta x = \Delta z$ the grid size (see x and z definitions in figure 3). This value and a discretization $\Delta x = \Delta z \simeq 0.04f$, with f the model freeboard, have been used for the simulations presented in § 4.

4. Physical investigations

In the following sections, the water-on-deck investigation carried out in Greco *et al.* (2005) is continued by comparing the experimental results with the full BEM and the DD–DC solvers. In both cases, the experimental wavemaker time history is used for the numerical wavemaker.

4.1. *Features of water shipping: initial plunging plus dam-breaking (PDB) event*

Most of the water-on-deck events observed during the experiments were characterized by an initial plunging phase followed by a dam-breaking water-shipping behaviour. These will be referred to as PDB events in the following discussion. An example of the initial and later stages of the water evolution when the vertical superstructure along the deck is considered in figures 4 and 5.

The figures refer to the first water on deck caused by nominal incoming waves $\lambda = 40f$ long and $H = 0.08\lambda$ high. A global physical discussion has been given

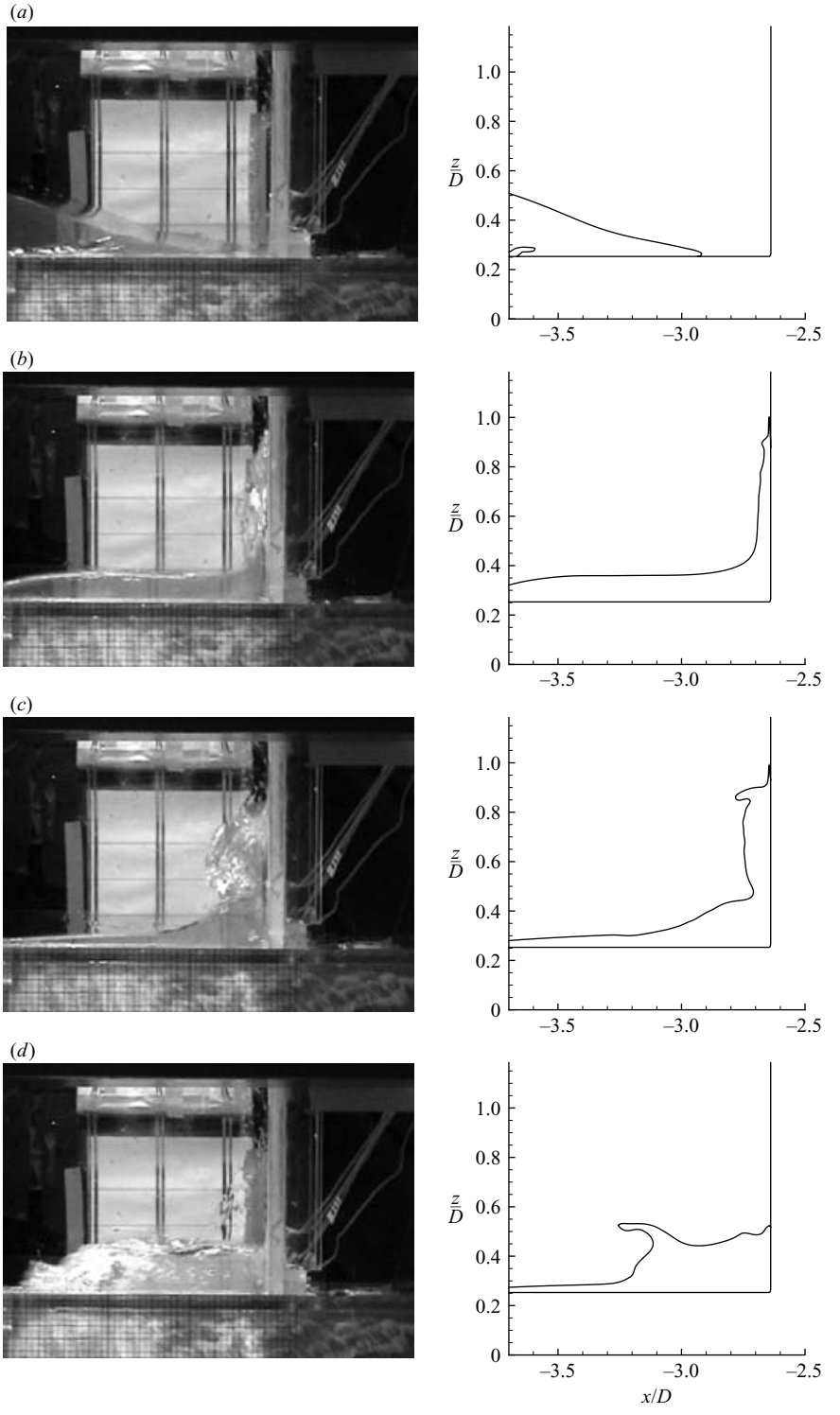

FIGURE 5. Initial plunging plus dam-breaking (PDB) type event: interaction with a vertical wall and later water evolution. Left: experimental snapshots. Right: DD–DC air–water interface. Time increases from (*a*) to (*d*) with time intervals of 0.16 s, 0.16 s and 0.12 s, respectively. Nominal incoming waves with $\lambda/f = 40$ and $H/\lambda = 0.08$.

in Greco *et al.* (2005) and will not be repeated, but additional relevant aspects will be investigated. In the figures the DD–DC results are compared with the experimental snapshots and show a good agreement globally. The BEM simulated the generation of the incoming waves and their interaction with the ship model up to the occurrence of the water shipping ($t \simeq 110\sqrt{f/g}$). The fluid domain was then split as shown in figure 3 and the later evolution was analysed through the coupling algorithm.

The numerical solution describes the plunging phase correctly without the need of an explicit condition at the deck edge, such as for instance condition A used for the BEM in Greco *et al.* (2005). However, it is not straightforward for a field solver to capture such localized phenomena because of the numerical smoothing. With the present method and because the body is fixed and aligned with the Cartesian grid, this has been achieved by narrowing the smoothing of the field variables across the body surface (at most inside one cell) and using a discretization $\Delta x = \Delta z \simeq 0.04 f$. In the case of a generic body, the smoothing should be extended further in terms of grid cells across the body to avoid stability problems, and the grid size should be adequately reduced to capture such flow details.

The DD–DC solver also predicts well the cavity entrainment caused by the impact of the plunging water with the deck. However some differences can be detected with respect to the thickness of the experimental fluid jet moving toward the bow (see figure 4*b*). One reason is that the thickness is comparable to the grid size used in the numerical simulation. Moreover, (i) surface tension and meniscus effects (at the flume glass) could play a role in the physical case; the view shown is rather localized, with the smallest grid dimension in the experimental images equal to 2 mm. Further, (ii) the use of a low-speed video camera (25 frames per second) involves an ambiguity when identifying the time instants of the images. Aspects (i) and (ii) reduce the importance of the small disagreements between the two results and support the capabilities of the numerical solver.

The numerical solution does not capture correctly the collapse of the cavity into bubbles (see figure 5*a*). However this phenomenon represents, in general, a challenging task for the numerical solvers. Further, the process of cavity disintegration is very sensitive to the environmental conditions and is associated with three-dimensional flow instabilities in the model tests. Without any numerical treatment, at a later stage the numerical cavity would detach from the 'deck' and follow the main flow. However, because of the assumption of incompressible air, it would be larger and remain longer in water than in the physical case. So, the numerical cavity was enforced to disappear artificially when the physical cavity fragmented into bubbles. This was obtained by simply substituting the air inside the cavity with water at the time instant when the cavity started to split into smaller cavities ($t \simeq 113.85\sqrt{f/g}$).

The agreement with the experiments also remains globally satisfactory during the water interaction with the vertical superstructure on the deck and the later water-off-deck phase, though the validation on a local scale is difficult when three-dimensional flow instabilities occur in the model tests (from figure 5*b*). These are well established during the water rising up the vertical wall on the deck and characterize both the jet tip and the bubbles reaching the superstructure (see figure 6).

Despite the three-dimensional effects, the model tests and the numerical solution show similar backward plunging jets during the water fall caused by gravity (figure 5*c*). The impact of such jets on the underlying water induces a splash up, accelerating the water-off-deck phase. This is evident in the numerical simulation while it can barely be seen in the experimental pictures due to the large amount of spray at this stage

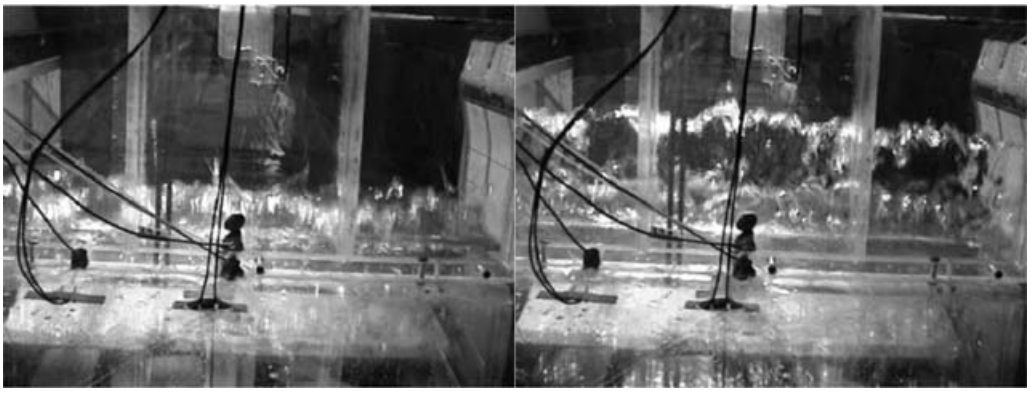

FIGURE 6. Growth of three-dimensional effects during the water rising up the vertical wall. View towards the incident waves. Time increases from left to right and the time interval is $\Delta t = 0.08$ s.

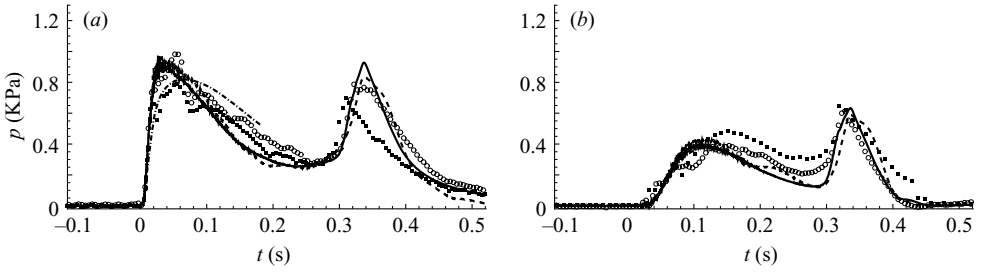

FIGURE 7. Initial Plunging plus dam-breaking (PDB) type event: pressure evolution along the vertical wall, respectively, at $0.24f$ (*a*) and $0.64f$ (*b*) above the deck. Symbols: two test runs (respectively open circles and filled squares); dash-dotted lines: full BEM results; solid lines: DD–DC results; dashed lines: DD–DC results without avoiding the cavity formed at the initial stages of the water shipping. Nominal incoming waves with $\lambda/f = 40$ and $H/\lambda = 0.08$. Here $t = 0$ indicates the time instant when a non-zero pressure is recorded at the lowest probe.

(figure 5*d*). The formation of spray is not handled by the method and its description is in general an issue for numerical solvers.

The green-water loads experienced by the vertical wall as a consequence of the interaction with the shipped water are analysed in figure 7 in terms of pressure time histories at two locations along the superstructure. As reported in Greco *et al.* (2005), the global behaviour has a double-peaked trend, similar to the 'church roof' behaviour described by Peregrine (2003), with the two peaks related, respectively, to the initial water-wall impact and to the later action of water falling under gravity.

Both the full BEM and the DD–DC solvers agree well with the experiments and the differences are comparable with those between the two test runs reported. The potential-flow solver predicts a slightly gentler pressure rise at the probe closer to the deck. The water fronts, numerically predicted by the BEM and DD–DC solvers, reach the wall as local half-wedges approximately with similar shapes. However, in the DD–DC simulation, very locally near the deck the tip of the water front has a blunt shape with a higher slope than the liquid wedge (see figure 5*a*). This leads to an initial blunter impact, so that the rise time of the pressure at the pressure gauge closer to the deck is shorter with the DD–DC simulation than with the BEM solver.

The zonal approach is able to capture the pressure evolution during the whole process of the water–wall interaction. This is not true for the BEM solver.

Figure 7 also gives the pressure evolution predicted at the two probes by the DD–DC solver when the initial cavity does not vanish artificially. The evolution of the numerical bubble, once sufficiently close to the vertical wall, is responsible for some oscillations in the loads. This suggests that the small oscillations visible in the experimentally measured pressure could be due to the motion of bubbles near the superstructure.

Analysing the entire water-on-deck event, the experiments highlighted three stages that could be relevant for green-water loads: (i) the air entrainment caused by the initial plunging near the bow, (ii) the impact of the water on the vertical superstructure, and (iii) the later water run-down under gravity and the consequent impact of a backward plunging jet onto the underlying water on the deck. These stages could be important in the design, respectively of the deck, the superstructures, and their combination.

Because no pressure measurement device was placed on the deck, the zonal strategy has been used to investigate the importance of the three stages. The time instants with the largest numerical pressures occurring for each are given in figure 8. The highest values have been recorded during phase (ii). Large pressures should occur locally and during a very small time period when the plunging wave, with a blunt tip, hits the deck during stage (i) but the DD–DC solver is not able to detect those fine details; this is a general challenge for all the numerical methods.

The solver models the air as an incompressible fluid, and this limits the reliability of the calculated pressure when bubbles are entrapped in the liquid. As shown in Greco *et al.* (2005), the pressure due to the air cushioning during phase (i) could represent a problem in terms of deck safety when translated by Froude scaling for instance to a full-scale FPSO (draft $D = 18$ m and maximum allowable overpressure of 60 KPa on the deck). The importance of air cushioning was also documented by Peregrine (2003) during the impact of breaking waves on a flat wall and by Walkden *et al.* (2001) during wave overtopping on caisson breakwaters with trapped air pockets.

Figure 8(*iii*) highlights the presence of a region 'lp' with local low pressure. The results for the vorticity field (not reported here) show that this is connected with a vortical structure formed near the foot of the vertical wall and rising in time. The occurrence of a similar low-pressure region would explain the presence of the bubbly area visible near the corner between the deck and the vertical wall in the model tests (see figure 5*b, c*). A lower pressure could have caused the surrounding bubbles to move toward the core of the vortical structure and coalesce, as suggested by some experimental pictures and by the oscillating pressure records.

4.2. *Features of the water shipping: hammer-fist (HF) type event*

The model tests also highlighted the occurrence of another unusual type of water-on-deck event not documented in the past. The related water shipping is shown in figure 9, which refers to the second water-on-deck event caused by nominal incoming waves with $\lambda/f = 30$ and $H/\lambda = 0.07$. The water reaches the ship deck in the form of a fluid arm with unchanged direction and thickness (L_{HF} in the figure) until gravity starts to play a role. The water block impacts the ship deck bluntly as in the 'Hammer Fist' karate strike. Therefore such an event will be referred to as HF-type water on deck in the discussion.

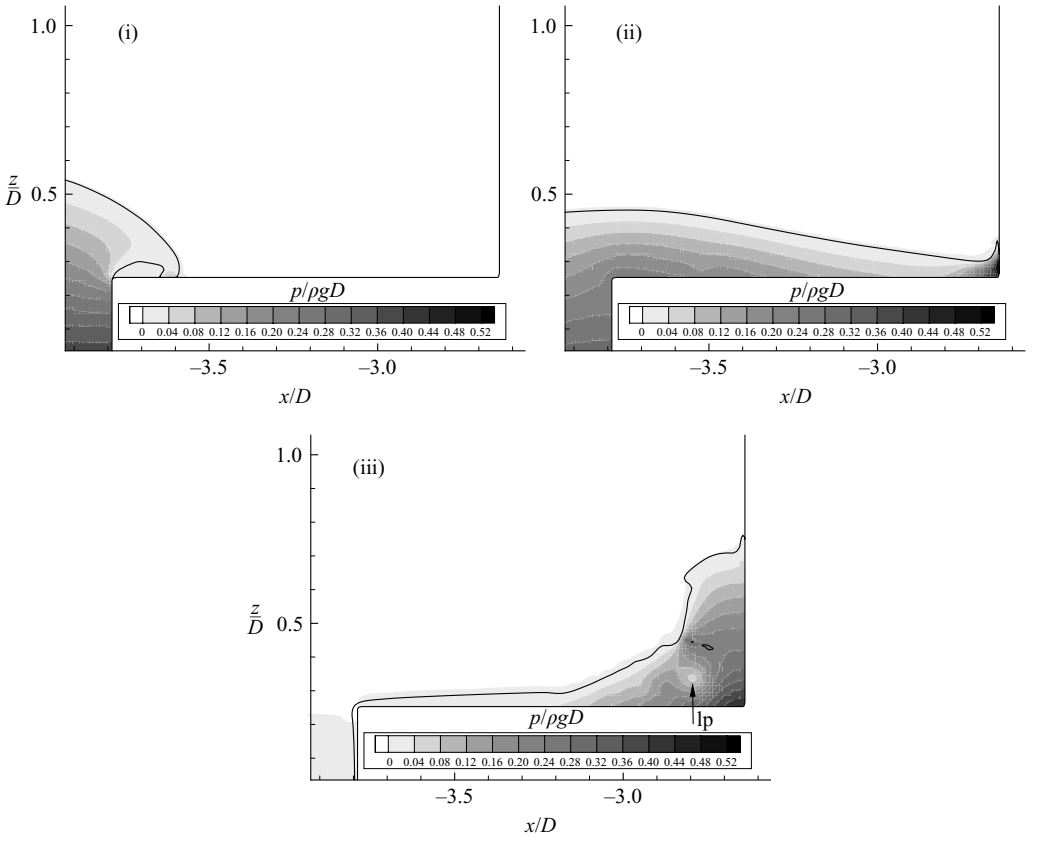

FIGURE 8. Initial plunging plus dam-breaking (PDB) type event: DD–DC pressure field. Phase (i), initial plunging phase and air entrainment ($t = 112.35\sqrt{f/g}$); phase (ii), water–wall impact ($t = 115.34\sqrt{f/g}$) and phase (iii), water run-down and water-water impact due to a backward plunging jet ($t = 119.61\sqrt{f/g}$). lp stands for the region of low pressure. In each plot the black solid line indicates the air–water interface. Nominal incoming waves with $\lambda/f = 40$ and $H/\lambda = 0.08$. $t = 0$ represents the starting of the wavemaker motion.

In this case the impact with the deck starts near the fore bow and affects a relatively large portion of the deck. An important question is why this phenomenon occurs. According to our investigations, an HF event is connected with steep waves.

For the nominal incoming wave parameters considered, the first almost irrelevant water shipping was caused by a broken wave (see figure 13*b*, below). The tendency to break was indicated by the full BEM simulations, as shown in figure 10(*a*). Micro-breaking of the leading waves was recorded experimentally. In the model tests, it is reasonable that the breaking reduced the kinetic energy of the waves approaching the bow and caused vorticity generation. The air–water mixture shown by the experimental upper layer of water (see left-hand plots of figure 9) could be the result of these events.

The BEM algorithm does not handle the breaking, but its predicted free-surface deformations agree fairly well with the model tests (see e.g. figures 9 and 13), perhaps because the damping effect connected with the breaking is approximately recovered by the numerical regridding. The second water-on-deck event, that is the HF, was due to a steep but not breaking wave. As this wave approached the model, the tendency of the wavefront to steepen was counteracted by the rise of the trough at the bow. This

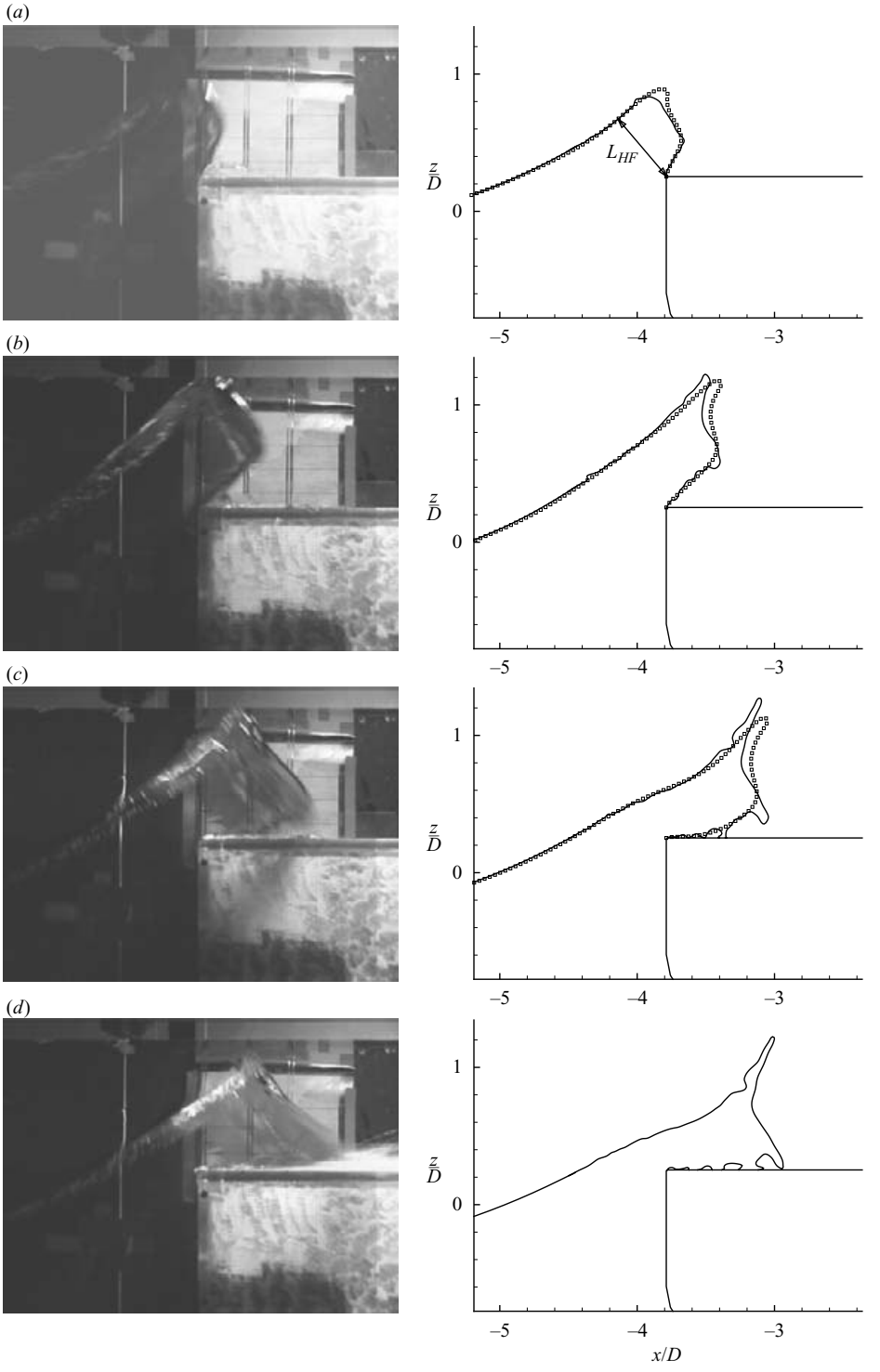

FIGURE 9. Hammer-fist (HF) type event: evolution of the shipped water. Left: experimental snapshots. Right: full BEM (squares) results by enforcing condition A at the deck (see Greco *et al.* 2003), and DD–DC (solid lines) air–water interface. Time increases from (*a*) to (*d*) with time intervals of 0.08 s, 0.08 s and 0.04 s, respectively. Nominal incoming waves with $\lambda/f = 30$ and $H/\lambda = 0.07$.

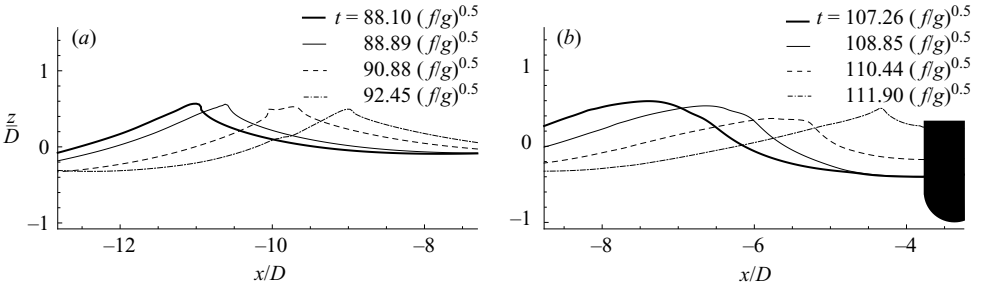

FIGURE 10. BEM free-surface evolution for the case with nominal incoming waves with $\lambda/f = 30$ and $H/\lambda = 0.07$. (*a*) Incipient free-surface breaking predicted by the full BEM and avoided by the numerical regridding. (*b*) Wave in the incoming system that will cause the Hammer-fist (HF) type event. $t = 0$ indicates the time instant when the wavemaker motion started.

supported a partial focusing of the water flow near the ship model (see figure 10*b*). The wave evolution resulted in a pronounced local behaviour near the vessel.

When passing the probe in front of the bow, the wave causing the HF event showed a maximum wave elevation similar to that causing the first water-on-deck event for the case with $\lambda/f = 40$ and $H/\lambda = 0.08$. However, locally near the deck-edge the flow conditions were rather different, as shown in figure 11(a, b) at the time instants when the water reached the freeboard.

For the PDB event, the air–water interface appears quite flat and nearly horizontal. The velocity field is rather uniform and mainly parallel to the bow front. In the HF case, instead, the interface has a local trough at the bow and a maximum at a distance of about $2f$ upstream of the bow. The intensity of the velocities is more than twice that for the PDB case. Further, the velocity vectors deviate substantially from the vertical direction at the wave crest and the flow is directed toward the ship deck.

The later evolution of the free surface is shown in figure 9 where the full BEM with condition A (see Greco *et al.* 2005) and the DD–DC solver results are compared with the model tests snapshots reported in the left. In the zonal strategy the BEM has been switched with the DD–DC solver just before the second event occurred ($t \simeq 111\sqrt{f/g}$). The full BEM and the DD–DC results agree satisfactorily with each other and are consistent with the experiments. However a detailed comparison with the experiments is not possible: owing due to light errors in the images, the low frame rate of the video camera and the large flow velocities involved, the water evolution was not precisely captured.

The main differences with the model tests are concentrated at the top, where the two numerical solutions show the formation of a thin layer of water with high velocity, i.e. a jet flow, not visible in the experiments. Despite the high curvatures and the small spatial scale involved, this difference does not seem to be due to surface tension. When introduced in the full BEM simulation (not shown here), surface tension did not prevent the formation of the jet. A possible explanation for this discrepancy could be connected with the wave breaking phenomenon that experimentally preceded the event, as discussed above, but was not modelled in the numerics. Alternatively it could be associated with the formation of spray during the development of the jet. In any case, the details of the jet do not affect the water interaction with the deck and the features of the water-deck impact are captured well by both numerical solvers.

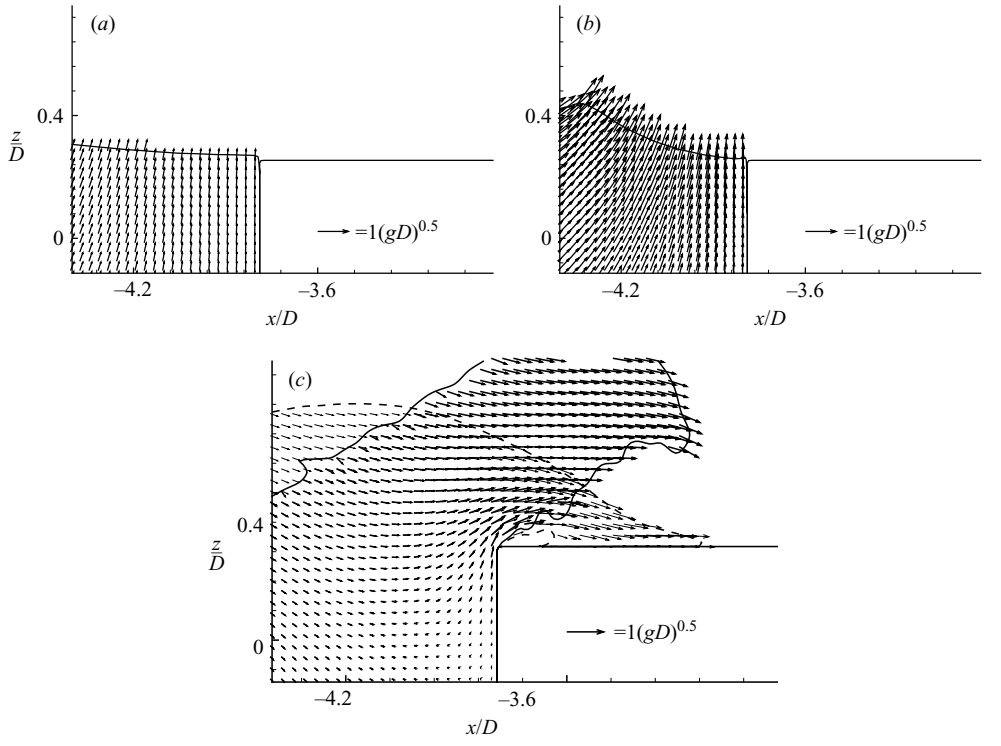

FIGURE 11. Air–water interface and flow velocities predicted by the DD–DC. (*a*) PDB event due to nominal incoming waves with $\lambda/f = 40$ and $H/\lambda = 0.08$. $t = 110.6\sqrt{f/g}$. (*b*) HF event due to nominal incoming waves with $\lambda/f = 30$ and $H/\lambda = 0.07$. $t = 111.9\sqrt{f/g}$. (*c*) PDB event (dashed line for the interface and thin vectors, $t = 113.5\sqrt{gf}$) and HF event (solid line for the interface and thick vectors, $t = 114.4\sqrt{gf}$). $t = 0$ represents the starting of the wavemaker motion.

In figure 9 the BEM free surface appears smoother than the air–water interface from the zonal approach. This is partially due to the regridding enforced dynamically during the BEM simulation. The regridding can also explain the slightly different shapes of the jet tips predicted by the two solvers. The DD–DC results show oscillations developing on the front of the fluid fist. Because of such oscillations the blunt impact with the deck causes the entrapment of small cavities.

The numerical origin of the oscillations has been checked by reducing first (i) the time step and then (ii) the grid size. In both cases the reduction factor was chosen equal to 1.5 to avoid links with the original discretization. Some differences were observed only for simulation (ii), as expected because of the local flow details examined and the sensitivity of the shedding process from the body discretization near the deck edge. However, in this case also the solution was characterized by oscillations with wavelengths similar to those predicted by the original discretization. These studies support the physical nature of the oscillations.

Because the heavier fluid is above the lighter one during the evolution, the oscillations may be related to a Rayleigh instability (see e.g. Birkhoff 1962). The physical mechanism introducing the growing perturbations is represented by the vorticity shed from the deck edge. Because the vortex shedding itself is subjected to Helmholtz instability (see e.g. Birkhoff 1962), the two types of instability are probably combined

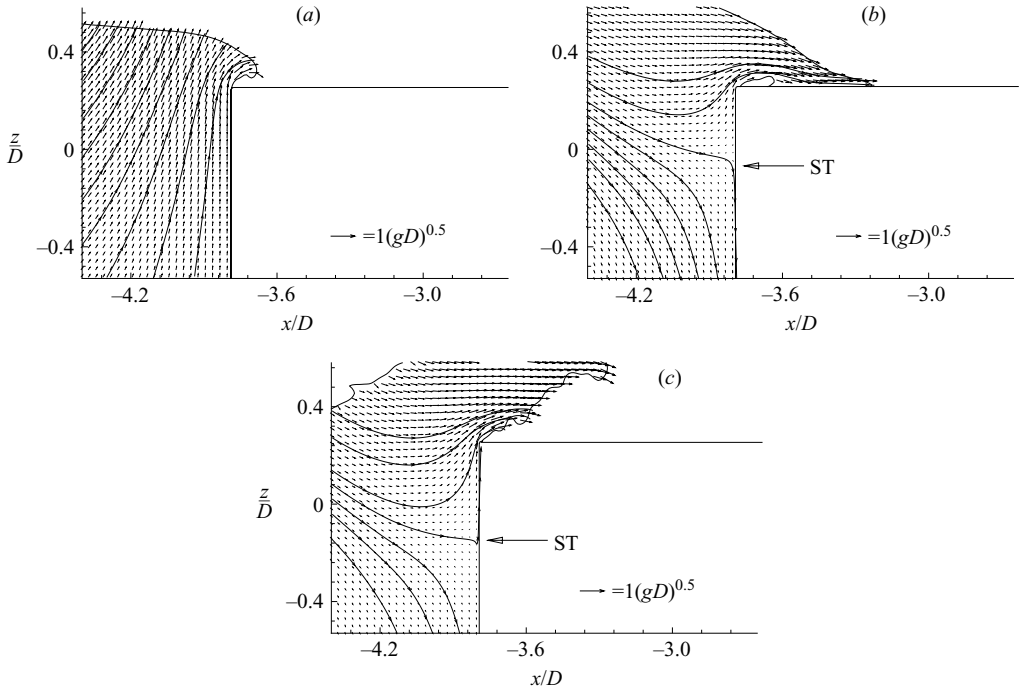

FIGURE 12. Air–water interface flow velocities and trajectories of the water particles as predicted by the DD–DC. (a,b) PDB event due to nominal incoming waves with $\lambda/f = 40$ and $H/\lambda = 0.08$ at $t = 111.8\sqrt{gf}$ and $t = 113.5\sqrt{gf}$, respectively. (c) HF event due to nominal incoming waves with $\lambda/f = 30$ and $H/\lambda = 0.07$ at $t = 114.4\sqrt{gf}$. $t = 0$ represents the starting of the wavemaker motion. In the plots, when visible, the position of the stagnation point (ST) along the bow front is indicated.

in this case, as suggested by the DD–DC results for the evolutions of the vorticity in water and of the air–water interface (not shown here).

Because the wavelengths involved are of the order of 1 cm at the model scale, the oscillations could be reduced by surface tension in the model tests. However, the quality of the experimental pictures prevents a deeper investigation. A numerical investigation of the surface tension effects at the model scale has not been performed here. In any case the unstable behaviour is expected to characterize the evolution at full scale.

Like the PDB-type event, during the HF event one can also distinguish three evolution phases before the water impacts the deck, dominated respectively by: (i) pressure gradient, (ii) pressure gradient and gravity, (iii) gravity. However, the different 'initial' conditions, i.e. when the water reaches the freeboard, lead to rather different features of the water–deck impact. In the HF case the 'initial' velocity field is generally diverted toward the ship deck (figure 11b) so that the impact starts from the deck edge, while in the PDB case it is almost vertical (figure 11a) leading to the formation of a plunging jet impacting on the deck.

Figure 11(c) shows the time instants when the two water-on-deck phenomena are characterized by very similar (both in direction and value) velocities off the deck. In the PDB case the shipped water has already hit the deck, while the impact has not yet occurred for the HF event. Analysing the two cases in terms of the stagnation point along the bow front shows that the stagnation point rises relatively more slowly in the PDB case than HF (compare figures 12a and 12c and remains far from the

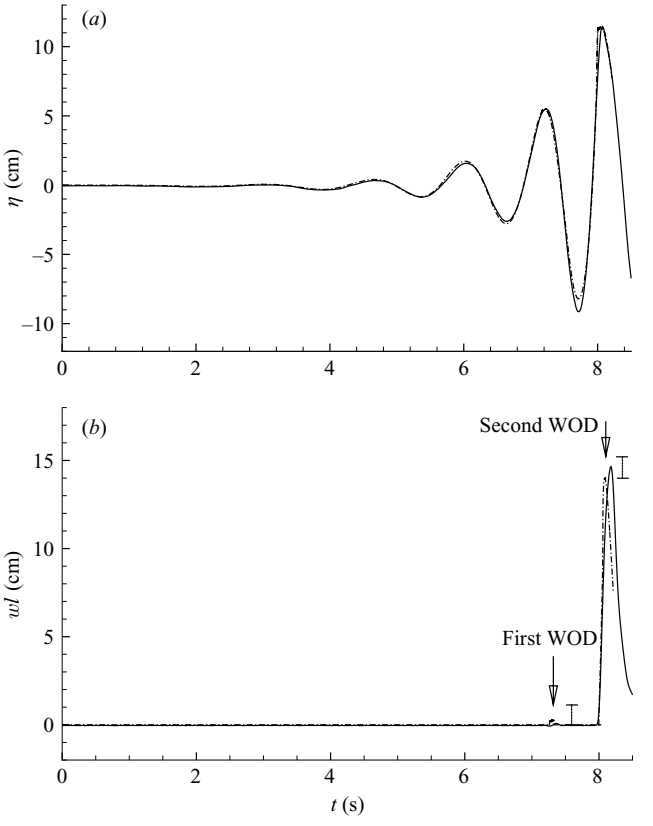

FIGURE 13. Hammer-fist (HF) type water on deck: time evolution of (a) the wave elevation η at $2.08f$ upstream of the bow and (b) of the water level on deck wl at the bow. Solid lines: experiments. Dash-dotted lines: full BEM results. The error bar arising from the measurement of the maximum freeboard exceedance is also shown (segment between horizontal solid lines). Nominal incoming waves with $\lambda/f = 30$ and $H/\lambda = 0.07$. WOD means water-on-deck event.

deck edge during the whole water–deck pre-impact phase. As a result, the flow can develop as a plunging wave with cavity closure at the impact against the deck (see figure 12a, b).

A more quantitative comparison of the numerical results with the experiments is shown in figure 13 in terms of the wave elevation in front of the bow and of the water level at the bow as functions of time. Only the full BEM results are given since they are practically identical to the DD–DC time histories. From the wave elevation results, at the later stages the numerics predicts slightly steeper waves with shallower troughs. The differences can be partially explained by the difficulties in the probe following the evolution of waves breaking in the physical flume. On the other hand the numerics has suppressed the breaking phenomenon because of the regridding.

Despite these aspects the agreement is reasonable and the same is true for the water level at the bow. In particular, the numerics is able to capture both the first small water shipping and the second one with differences which are within the experimental uncertainty. For this purpose, the error bar for the measurement of the maximum freeboard exceedance is also shown in the figure 13(b). Because only one test run was done for this incoming-wave case, the error bar was estimated by using the repeatability tests for the case discussed in the previous section.

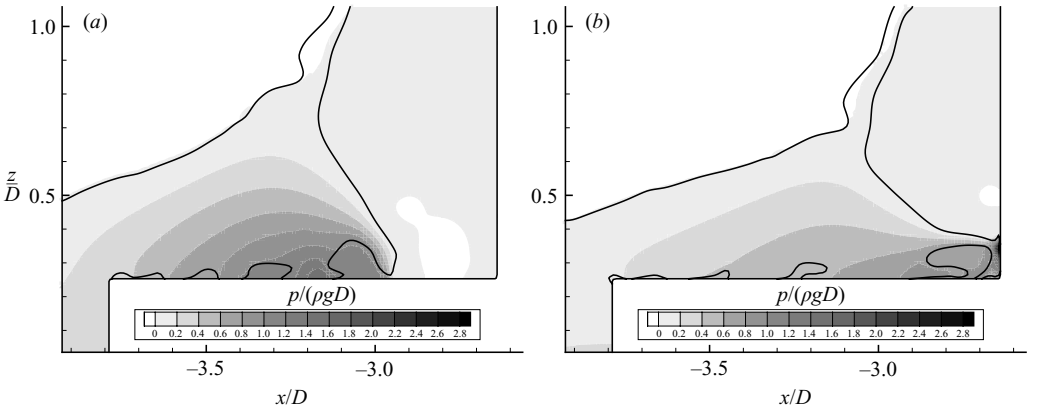

FIGURE 14. Hammer-fist (HF) type water on deck: evolution of the pressure field as predicted by the DD–DC. Nominal incoming waves with $\lambda/f = 30$ and $H/\lambda = 0.07$. (*a*) $t = 115.48\sqrt{gf}$. (*b*) $t = 115.93\sqrt{gf}$. The solid line in each plot gives the air–water interface. $t = 0$ represents the starting of the wavemaker motion.

Figure 9(*d*) shows the water–deck post-impact phase. At this stage the full BEM solution is no longer applicable. Experimentally very large velocities occur leading to significant spray formation at the tip of the water flow developing along the deck. The DD–DC simulation is not able to capture the spray but predicts well the impact process and records velocities larger than $4\sqrt{gf}$ (or $2\sqrt{gD}$) along the deck. Water front velocities equal to $2\sqrt{gD}$ in a fully developed (i.e. in shallow water) dam-breaking flow (see e.g. Stoker 1958) would imply a water height of the initial reservoir equal to the vessel draft.

The incoming-wave case causing this water-on-deck event was studied experimentally without any vertical superstructure on the deck. Further, as usual for the present model tests, no pressure device was placed on the physical deck. Therefore the DD–DC solver has been used to investigate the green-water loads induced on the deck and on a vertical deck superstructure. The results of this analysis are discussed next.

A vertical superstructure was introduced on the deck, as in the water-shipping case analysed in the previous section, and the evolution of the pressure field analysed (see figure 14). The maximum pressures recorded on the deck are much larger than those connected with the water interaction with the deck discussed in the previous section. If translated by Froude scaling to a full-scale FPSO ($D = 18$ m), such loads would correspond to the hydrostatic pressure given by a column of water 30 m high, while the full-scale nominal incoming-wave period and height are 9.35 s and 9.55 m, respectively.

From the features of the impact with the deck, i.e. the relevant loads are connected with rather blunt water–deck impact, one can expect that, when going to the full-size case, three-dimensional effects would play a minor role in reducing the maximum loads compared to the two-dimensional predictions. At impact the pressures are non-uniform but high along a large portion of the deck with loads greater than the hydrostatic pressure given by a column of water 10 m high (at full scale) over a distance of about $0.65D$.

Because of the impact features and the large amount of shipped water, the loads remain high (greater than the hydrostatic pressure given by a column of water of 8 m)

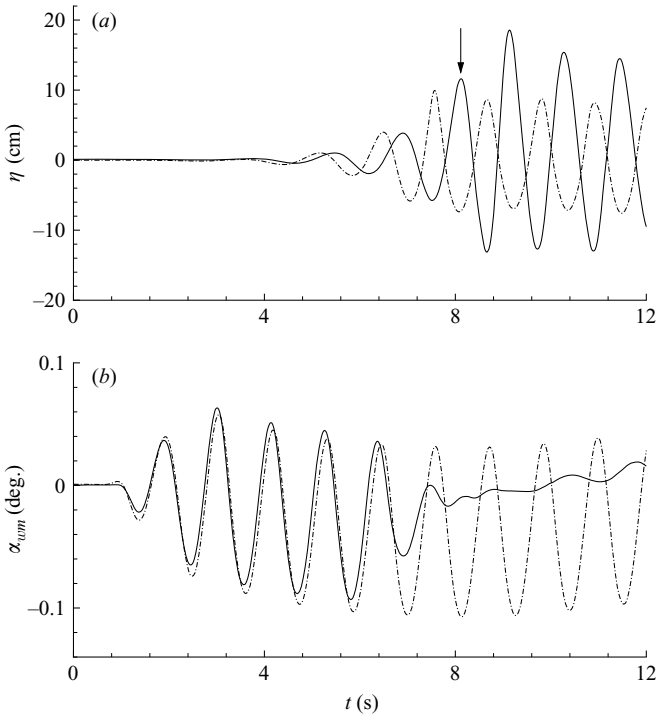

FIGURE 15. (*a*) Time history of the wave elevation measured by the probe about $2.08f$ upstream of the bow. Dash-dotted line: case without ship model in the flume. The duration of wavemaker motion ensured the establishment of steady-state conditions. Solid line: case with the ship model. The wavemaker motion stopped after few periods. The first water-on-deck event is caused by the leading wave (arrow in the plot). (*b*) Time histories of the corresponding wavemaker motions.

during the whole water-shipping event. The pressures involved could be important for structural stresses, but a further investigation of the stresses is beyond the scope of the present research and would require knowledge of the deck structural details. For this type of water-on-deck event the interaction with the vertical wall is more complex than for a PDB event, with the largest pressure values not simply localized at the foot of the superstructure.

4.3. *Wave parameter analysis*

The nominal incoming waves are only weakly related to the actual incoming waves experienced by the model, both for the first water-on-deck event and for the following ones. This is shown by figure 15(*a*) in terms of the time history of the wave elevation at the probe close to the bow (about $2.08f$ upstream, see figure 3) with and without the ship model and for the case of incoming waves with $\lambda/f = 40$ and $H/\lambda = 0.08$.

The first event is caused by the leading wave (indicated by the arrow in the plot) which is steeper than the following waves in the wavetrain and is increased by about 22% due to the presence of the body. The difference from the nominal incoming system is more pronounced for the following crests since they are much more affected by the reflection from the body and are modulated due to the stopping of the wavemaker after few periods (see figure 15*b*). As a result, (i) the generated disturbances appeared similar to irregular wave systems approaching the ship and (ii) waves in the same wavetrain caused water-on-deck events of different severity

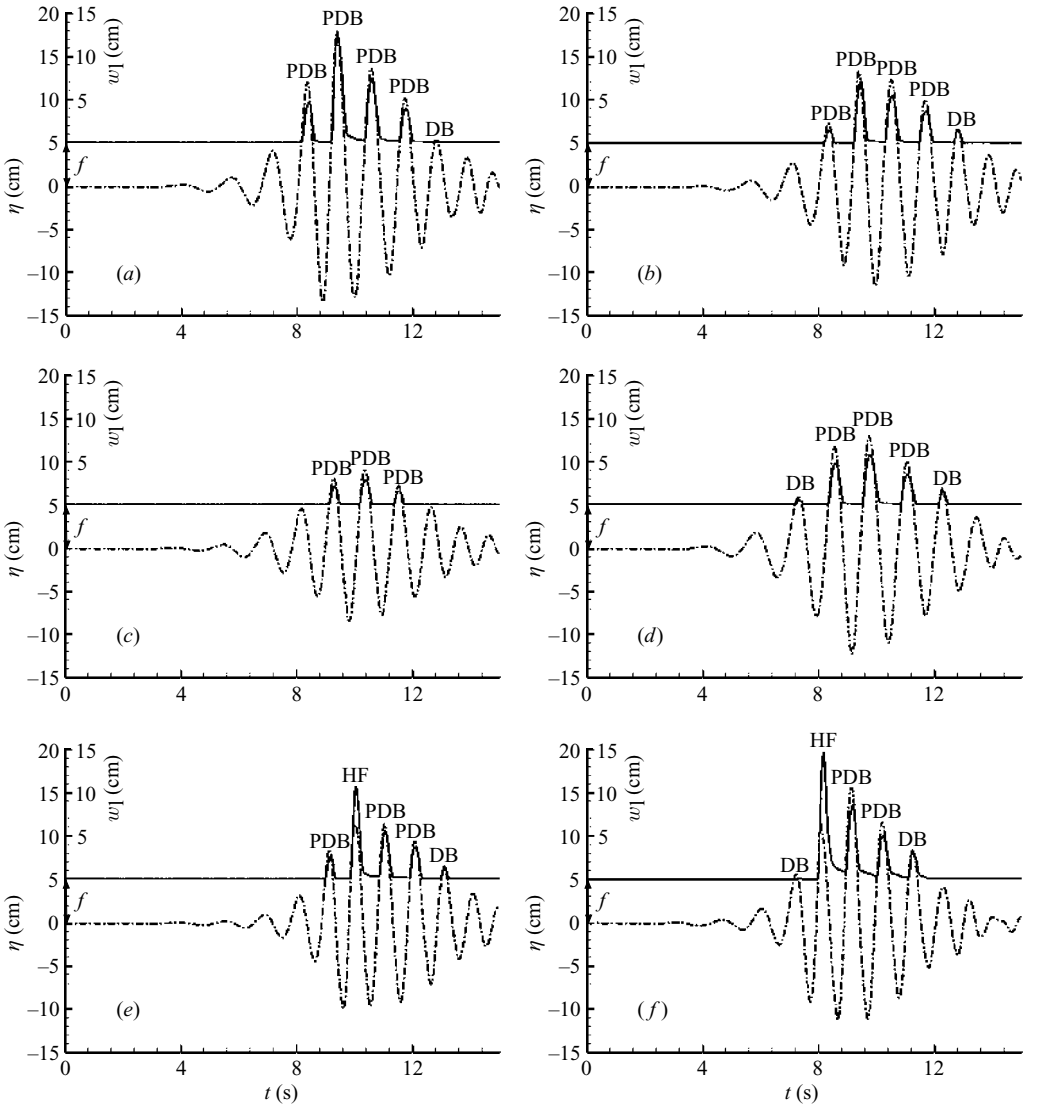

FIGURE 16. Evolution of the wave elevation at $2.08f$ upstream of the bow (η, dash-dotted lines) and at the bow ($f + wl$, solid lines). Nominal incoming waves with $\lambda/f = 40$ and $H/\lambda = 0.08$ (*a*), $\lambda/f = 40$ and $H/\lambda = 0.06$ (*b*), $\lambda/f = 40$ and $H/\lambda = 0.04$ (*c*), $\lambda/f = 50$ and $H/\lambda = 0.06$ (*d*), $\lambda/f = 30$ and $H/\lambda = 0.06$ (*e*), $\lambda/f = 30$ and $H/\lambda = 0.07$ (*f*). DB = dam-breaking type water on deck. PDB = initial plunging phase plus large-scale dam-breaking type water on deck. HF = hammer-fist type water on deck. No superstructure was placed on the deck.

and type. Both these aspects are investigated in figure 16 where the time evolution of the wave elevation, η, measured in front of the ship bow is plotted together with the elevation reached by the water at the bow, that is $f + wl$ (see figure 1), for experiments without a vertical superstructure on the deck.

If $wl > 0$ there is water shipping, so the comparison of η and wl time histories allows us to identify in each wavetrain the incoming waves causing the water-on-deck occurrence. Because the larger wl is, the greater the mass of shipped water, it is also possible to classify these waves in terms of the green-water severity. Further, we can

relate them to the different main types of water shipping, as indicated in figure 16. This has been done using the video recordings of the experiments.

From the analysis, PDB represents the most common type of event observed in the model tests. In this case the water elevation η relative to the mean free surface reached higher maximum values than the wave elevation recorded at the bow.

Some of the events characterized by a small amount of shipped water did not show any visible tendency of the water to plunge onto the deck and therefore they have been classified as dam-breaking (DB) events. For these the maximum wave elevation at the bow is practically identical to the one recorded upstream. This suggests that the occurrence of a DB event is not only related to a very small spatial scale (relative to the ship freeboard) but it can also be connected with waves 'long' with respect to the ship's freeboard. In the latter case the water run-up along the bow and the related vertical velocities would be less affected by local interactions. This would counteract the formation of a localized plunging.

In the PDB case, the local interaction is more relevant so that the position of maximum wave elevation is shifted with respect to the bow. The minimum ratio between the $\eta_{\max}$ measured at $2.08f$ upstream the bow and $(wl+f)_{\max}$ for which a PDB event has been recorded in the experiments was about 1.04.

The occurrence of the maximum wave elevation at the bow in the DB events counters the development of a plunging phase since it implies that the deck edge becomes a stagnation point when gravity starts to matter. This is consistent with the fact that air entrainment is avoided when the stagnation point along the bow gets close to the deck edge before gravity plays a major role above the deck (see discussion in § 4.2).

The previous observations suggest that another possible way to cause DB events is associated with horizontal velocities large compared with the vertical ones, since also in this case the deck edge could become a stagnation point. Both for the PDB and DB events the time duration of the water shipping remains close to the time interval for the incoming wave to exceed the freeboard, i.e. $\eta \geqslant f$.

The tests also recorded the occurrence of two HF events. These are characterized by flat impact without apparent air entrapment near the bow. We should stress that this is the first documentation of such a kind of water-on-deck event, despite the large numbers of water-on-deck experiments performed in recent decades. Therefore, the detection of two HF events should not to be considered as a limit of the physical investigation, but actually a fortuitous chance to look for common features and to detect possible conditions supporting the occurrence of such events, as discussed next.

For the recorded HF cases, $(wl+f)_{\max}$ is much larger than $\eta_{\max}$ of the related incoming wave. As a result, the duration of water shipping is apparently greater than the time interval for the incoming wave to exceed the freeboard. During an HF event the maximum wave elevation is reached somewhere on the deck due to the formation of a fluid arm (water block) eventually hitting the deck. So, the experiments suggest that the location of the maximum wave elevation moves from the deck to the bow and then to the sea on going from the HF to the DB and then to the PDB event. This trend is consistent with the increase of wave reflection by the ship on going from the HF to the DB and then to the PDB event, as observed in this and previous sections.

In the following the water on deck is analysed in terms of the incoming-wave parameters. This has been done by introducing the local definitions given in figure 17(*a*) which are more appropriate than the nominal (prescribed) ones because of the highly transient features of the flow in the model tests. The local parameters characterize each wave inside the wavetrain and therefore identify more

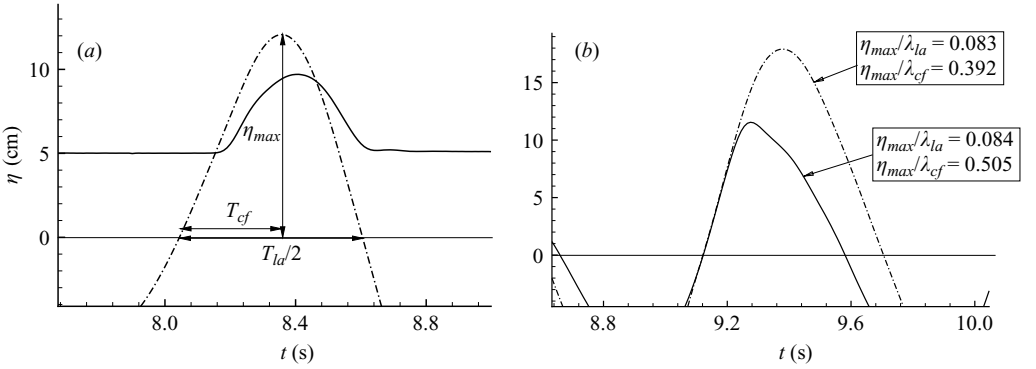

FIGURE 17. (*a*) Local incoming wave parameters $\eta_{\max}$ and T_{la}. Dash-dotted and solid lines represent the evolution of the wave elevation at $2.08f$ upstream of the bow, η, and at the bow $f + wl$, respectively. The case corresponds to the first water-on-deck event for figure 16(*a*). (*b*) evolution of η. Dash-dotted line: PDB type event, (second water-shipping for figure 16*a*). Solid line: HF event (second water-shipping for figure 16*f*).

realistically the incoming waves responsible for water shipping. This choice has also the advantage of increasing the number of wave cases useful for the analysis. In fact for each wavetrain one can identify about five 'local' waves causing water-on-deck events (see figure 16), characterized by different heights and slightly different wavelengths. Therefore they allow trends in the features of water shipping and effects of some important parameters to be investigated.

A possible choice of the wave steepness could be $\eta_{max}/\lambda_{la} = \eta_{max}/[gT_{la}^2/2\pi]$, which represents an average measure of the incoming-wave nonlinearities. In fact the waves approaching the ship model showed a more or less pronounced asymmetric time evolution when passing the wave probe upstream of the bow. This suggests a corresponding asymmetric (steep) wavefront. Examples of $\eta(t)$ time evolutions are given in figure 17(*b*) for two incoming-wave cases. The related curves have been synchronized to facilitate their comparison. In this context, a more appropriate definition of the steepness would be the so-called crest-front steepness $\epsilon_{cf} = \eta_{max}/\lambda_{cf} = \eta_{max}/[gT_{la}T_{cf}/2\pi]$ as applied by Kjeldsen & Myrhaug (1979) to define a geometrical criterion to predict wave-breaking phenomena.

The ϵ_{cf} values for all the cases considered are plotted in figure 18(*a*) and classified according to the type of water-on-deck event. The most severe PDB event is connected with a steepness slightly larger than the one characterizing the less severe HF event recorded. However, generally the crest-front steepness tends to increase on going from the DB to the PDB and then to the HF events.

The non-dimensional maximum vertical velocities at the probe upstream of the bow, W_w, and at the bow, W, are also reported in the same plot. They have been estimated by time differentiating the measured time histories for η and wl, respectively, and taking the maximum for each wave of interest inside the wavetrain. On average, W_w and W have the same trend as the steepness on going from the DB to the HF phenomena. For the DB events, the 'incoming wave' vertical velocity is clearly larger than the local value at the bow. The two velocities become closer for the PDB phenomena and their ratio is reversed for the HF cases.

From the discussion above, the 'local' incoming waves used for the present investigation are partially affected by the diffraction and reflection due to the body presence. However this does not diminish the findings and outcomes of the wave-parameter

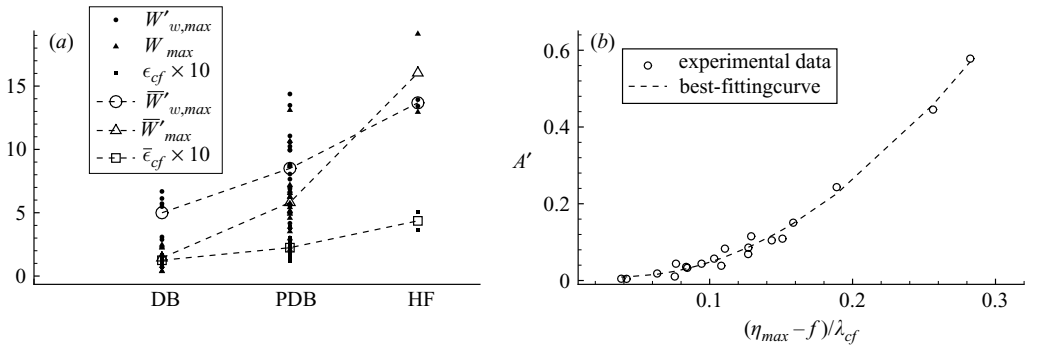

FIGURE 18. (*a*) Maximum vertical velocity connected with the local incoming waves, $W_{w,max} = (W_w)_{max} = (\mathrm{d}\eta/\mathrm{d}t)_{max}$, maximum vertical velocity at the bow, $W_{max} = (W)_{max} = (\mathrm{d}wl/\mathrm{d}t)_{max}$, and crest-front local incoming wave steepness, $\epsilon_{cf} = \eta_{max}/\lambda_{cf}$ ($\lambda_{cf} = gT_{la}T_{cf}/2\pi$), for all the events studied. $W'_{w,max} = W_{w,max}/\sqrt{gf}$, $W'_{max} = W_{max}/\sqrt{gf}$ and the above-line symbols represent the mean values obtained for the DB, PDB and HF water-on-deck events. (*b*) Initial area (A) of the entrapped cavity as a function of the modified incoming wave steepness (ϵ_{mcf}) for all the PDB cases. The best-fitting curve is $A' = 9.1760\epsilon_{mcf}^2 - 0.6437\epsilon_{mcf} + 0.0203$. $A' = A/f^2$ and $\epsilon_{mcf} = (\eta_{max} - f)/\lambda_{cf}$, with $\lambda_{cf} = gT_{la}T_{cf}/(2\pi)$.

analysis performed. The trends and links found, as well as the existence plane of the water-on-deck scenarios that can be drawn from them (see next section), are not affected by the fact that the 'real' incoming waves would be slightly less steep than the ones considered in this analysis. Further, the approach based on the use of such 'local' waves could be useful for investigating the water-on-deck event in a more general context of a real ship in irregular sea. For instance, performing the same type of probe measurements at full scale one could detect the water shipping and identify the types, estimate roughly their severity and build up short- and long-term statistics of the green-water phenomenon.

Figure 18(*b*) gives the initial area (A) of the cavity entrapped during the initial plunging phase for all the PDB events studied. This has been evaluated through image analysis of the experimental video recordings. When using this technique, the alignment errors of the video camera with the plane of the motion have not been corrected. However, because the air entrainment always occurred close to the deck edge, where the focusing point was set, the related errors in terms of cavity-area estimates are expected to be small. Another error source is the relatively small frame rate of the video camera (25 frames per second) that made it practically impossible to capture exactly the time instant of the water–deck impact. To overcome such a problem the closest time instant to the impact has been selected and the water evolution before and after the impact analysed to help the detection and estimation of the initial cavity. A final error source in the image analysis is associated with the light. In this context the use of a fluorescent material (Natrium flourisenium powder mixed with Dutch syrup) helped to distinguish the water from air.

Each cavity profile was estimated ten times to ensure that the errors in evaluating A were of the same order for all the cases studied. The area presented is the mean value of the ten estimations. In figure 18, A has been plotted against the 'modified' steepness $\epsilon_{mcf} = (\eta_{\max} - f)/\lambda_{cf}$, which was preferred to ϵ_{cf} because it is slightly better correlated with the data for the non-dimensional area $A' = A/f^2$. In particular, A' follows a parabolic behaviour, implying that both A' and its sensitivity to the steepness variations increases with ϵ_{mcf}.

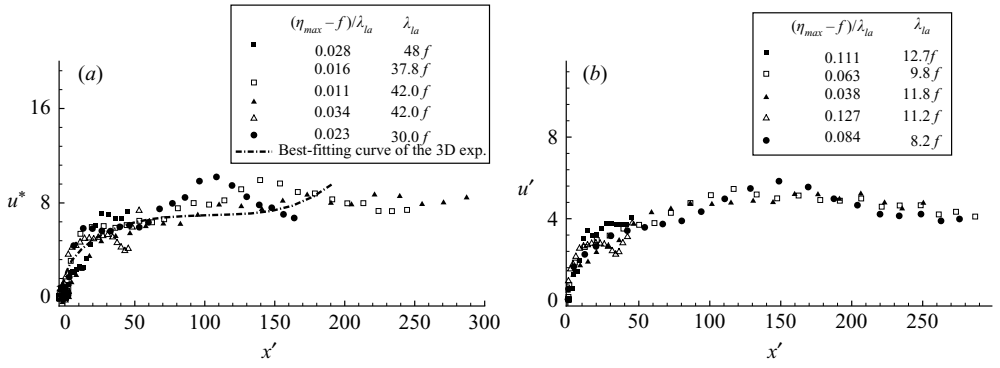

FIGURE 19. Velocity, u, of the water front along the deck as a function of the distance, x, from the bow during the first PDB water-on-deck events. (a) The variables are presented as $u^* = u/\sqrt{g(\eta_{\max} - f)\epsilon_{mla}}$ and $x^* = x/[(\eta_{\max} - f)\epsilon_{mla}]$, $\epsilon_{mla} = (\eta_{\max} - f)/\lambda_{la}$. The best-fitting curve for the three-dimensional water-on-deck experiments by Barcellona *et al.* (2003) is also shown, for which the corresponding non-dimensional variables are, respectively, $u/\sqrt{g(H-f)\epsilon_m}$ and $x/[(H-f)\epsilon_m]$ with $\epsilon_m = (H-f)/\lambda$ and the wave parameters defined from the wave packets, see Barcellona *et al.* (2003) for more details. (b) The variables are presented as $u' = u/\sqrt{g(\eta_{\max} - f)\epsilon_{mcf}}$ and $x' = x/[(\eta_{\max} - f)\epsilon_{mcf}]$, $\epsilon_{mcf} = (\eta_{\max} - f)/\lambda_{cf}$.

The results for the initial area can be transferred to full scale by Froude scaling. However, as pointed out in Greco *et al.* (2005), this cannot be done for the further evolution of the cavity, as then the Euler number $Eu = p_a/\rho V^2$ (where V is a characteristic velocity), governing the compressibility of the air in the cavity, must be considered. Analysing numerically the air cushion due to the wave impact on the bottom of a floating structure, Greco, Landrini & Faltinsen (2003) found that if the Euler number is large enough, say $Eu \sim O(10^3)$, the air in the cavity tends to escape, preventing the closure. Cavity entrainment occurs in the present experiments, implying a sufficiently small Euler number. In fact, $Eu \simeq 210$ if the impact velocity is used as reference velocity V.

Figure 19(a) gives the velocity, u, of the water front along the deck obtained by time differentiating wf measured during the first relevant water-on-deck events, i.e. causing a deck wetness with at least $0.0002\,\mathrm{m}^2$ of shipped water. It shows all the incoming wave systems studied except those responsible for the HF phenomena, implying that the events considered were of the PDB type. As a consequence, the estimated u corresponds exactly to the water front velocity only once the cavity collapse has occurred. Otherwise u is the wetting velocity of the deck, i.e. it also accounts for the water flow toward the deck edge during the impact of the initial plunging jet on the deck. The water-front velocity is plotted against the distance, x, from the bow. Consistently with the three-dimensional analysis carried out by Barcellona *et al.* (2003), the two quantities are presented as $u^* = u/\sqrt{g(\eta_{\max} - f)\epsilon_{mla}}$ and $x^* = x/[(\eta_{\max} - f)\epsilon_{mla}]$, respectively.

Barcellona *et al.* (2003) studied water shipping on three ship models with blunt bows using wave packets focused on the front of the bow as incoming-wave systems. The modified wave steepness was defined as $\epsilon_m = (H-f)/\lambda$, with H and λ being the wave height at the focusing point and the wavelength of the central wave component in the incoming wave packet, respectively. The logic behind the three-dimensional experiments is similar to that followed here, where $\epsilon_{mla} = (\eta_{\max} - f)/\lambda_{la}$ is a measure of each wave causing the event rather than the nominal wave system. With this

choice of the non-dimensional parameters, the velocity values for the different water-on-deck events become similar, suggesting the influence of wave nonlinearities also when shallow water conditions are established during the water propagation along the deck. Further, the present results are close to the best-fitting curve of the water-front velocities estimated along the ship centreline by Barcellona *et al.* (2003), also reported in the plot.

The agreement appears more evident when accounting for the differences both in terms of test conditions and procedures used to evaluate u. The velocity in the three-dimensional model tests was estimated through image analysis by taking the position of the water front along the centreline in any frame and approximating the time derivative with the incremental ratio, that is the velocity was evaluated as the ratio between the difference of two successive water-front positions and the time interval between them. From the comparison, despite the three-dimensional behaviour of the flow on the deck, a simplified two-dimensional model can be used to understand the flow features along the ship centreplane. This axis corresponds to one of the most severe directions in terms of shipped-water interactions with the deck and superstructures on it.

The velocities in figure 19(b) are made non-dimensional by using ϵ_{mcf} instead of ϵ_{mla}. The observations made above for the water-front velocities are still valid but now the curves almost fall onto a single curve, confirming the crest-front steepness as the relevant parameter in the present case.

4.4. *Scenarios connected with water shipping*

The present and previous water-on-deck studies by the authors (Greco 2001; Faltinsen, Landrini & Greco 2004; Greco *et al.* 2005) suggest that the 'green water' on deck is qualitatively associated with the scenarios given in figure 20. In particular one can have: dam-breaking (DB, plot a) type events characterized by flow of water along the deck similar to those generated by the breaking of dams; initial plunging plus dam-breaking (PDB, plot b) type events, where the dam-breaking water evolution is preceded by an initial plunging phase; plunging wave (PW, plot c) type events, with the occurrence of a large-scale plunging jet impacting on the deck and dominating the water-on-deck features; and hammer fist (HF, plot d) type events.

In the extreme cases flip-through phenomena (see e.g. Cooker & Peregrine 1992 and Lugni *et al.* 2005) could occur at the bow (plot e) leading to high localized pressures along the bow front and to the development of an upward fluid jet with large velocity. In these circumstances the bow-stem impact is of more concern for ship safety, while water on the deck can either be avoided by reflection from the ship, or result in a 'white water' type of event. In the latter case the deck is not impacted by compact masses of water, like in a green-water phenomenon, but mainly by spray which can cause difficulties and delays for the operations on board rather than being dangerous for the structural integrity.

The parametric plane of the water-on-deck scenarios in terms of the ratio W_w/W, between the incoming wave vertical velocity W_w and the vertical velocity W at the bow, and of the incoming wave steepness, say ϵ, is given in figure 20(f). W_w/W is used to characterize the local effect of the ship on the free-surface elevation, while ϵ is a measure of the incoming-wave nonlinearities.

DB events could exist in this plane for sufficiently small values of ϵ combined with high values of W_w/W. When the latter decreases, the probability of PDB phenomena rises and the same is true as the steepness increases. For a given ϵ one can avoid the

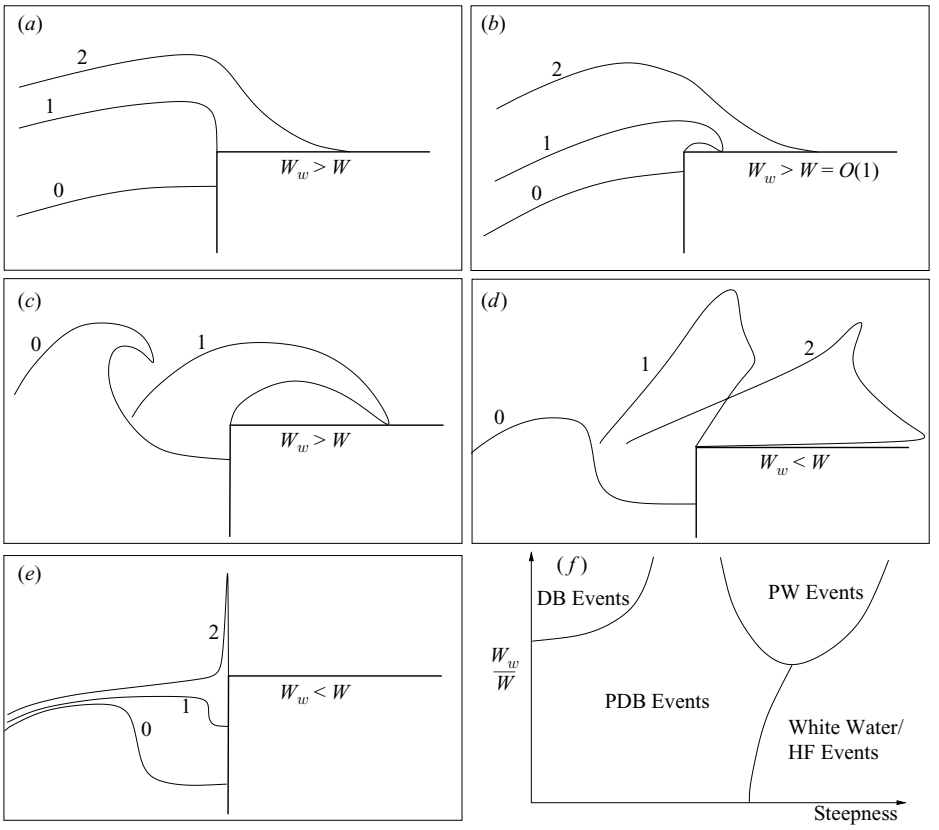

FIGURE 20. Scenarios of water shipping. (*a*) Dam-breaking (DB) type event, (*b*) initial plunging followed by a large scale dam-breaking (PDB) type event, (*c*) plunging wave (PW) type event, (*d*) hammer fist (HF) type event, (*e*) flip-through without water on deck or with 'white water'. The free-surface configurations are labelled with numbers increasing with the time. Plot (*f*) shows the scenarios in terms of the ratio between the incoming wave vertical velocity W_w and the vertical velocity W at the bow and in terms of the incoming wave steepness.

initial plunging phase by increasing W_w/W sufficiently, but a threshold value of this steepness will exist beyond which this is no longer possible.

When the ϵ increases, the spatial (and thus temporal) scale associated with the initial plunging phase will increase, and eventually will characterize the whole water-on-deck event (plunging-wave-type water on deck, PW). The large-scale plunging, rather than connected with the wave–body interaction, is the result of an incoming wave breaking onto the ship deck. However, the related features would obviously be affected by the presence of the vessel. The occurrence of a PW event implicitly requires a sufficiently large value of the velocity ratio since the plunging wave rise above the deck needs to be faster than the water run up along the bow.

When W_w/W decreases, the incoming waves tend to interact more severely with the bow. This is the region where *HF* events can be caused by a partial focusing at the bow between the incoming wavefront and the wave trough. Such an interaction can lead to a fluid fist hitting the deck like a hammer, as discussed in § 4.2. If the wave–body phasing is so that the wavefront and its trough focus at the bow, then a wave–bow impact happens, with the occurrence of a flip-through phenomenon.

Naturally this is a simplified analysis. The features of the shipped water depend also on other variables characterizing both the local flow conditions associated with the wave–vessel interaction and the incoming waves. This implies an investigation in a multi-dimensional space. For instance, here the relative horizontal velocity has not been considered although some comments have been made about it in § 4.3. However, the existence plane used in the present analysis would play an important role in classifying the features of the water-on-deck events.

5. Conclusions

The green-water problem has been investigated numerically and experimentally by studying water shipping on a two-dimensional fixed barge-shaped structure. Model tests by Greco *et al.* (2005) have been used to validate the numerical extension of the BEM solver performed in the framework of a DD–DC strategy.

In the zonal approach, the water on deck is analysed by an NS solver combined with an LS technique. The NS–LS domain contains the vessel and is surrounded by an outer domain solved by the BEM. Both solvers describe the air–water evolution and assume the two fluids as incompressible. The DD–DC strategy compared well with the experiments and with a full BEM solution and proved to predict correctly the green-water loads on a vertical wall placed on the deck.

The numerical tool was used to investigate further the water-shipping events tested by Greco (2001). Most of the water-shipping phenomena were characterized by an initial plunging phase followed by a global dam-breaking-type (PDB) behaviour, as discussed in Greco *et al.* (2005). These were associated with steep but not breaking incoming waves. A type of event, not documented before, has been detected in the form of a hammer fist (HF, water block) hitting the deck bluntly. It was connected with a steep incoming wave that was far from breaking. The green-water loads on the deck and along the vertical superstructure for these two types of phenomena have been investigated.

The HF event showed important loads on the deck connected with the initial water–wall impact while no conclusion can be drawn concerning the effect of the air entrainment on the initial plunging phase in the PDB case. To investigate this aspect a compressible model is required for the air. For both types of events the interaction with a vertical wall on the deck caused the highest loads.

The features of the water on deck for all the cases studied experimentally were discussed in terms of local incoming-wave parameters which are more appropriate than the nominal ones due to the transient behaviour of the tests. It was found that on going from a DB to a PDB and to an HF type event, the maximum wave elevation at the bow tends to become larger than the maximum incoming-wave elevation. Moreover, on average the incoming wave steepness, the maximum vertical wave velocity, W_w, and the maximum vertical velocity at the bow, W, increase. Also, W tends to become larger than W_w. These results are valuable in the more general context of investigating statistically the occurrence and severity of the green-water phenomena caused by irregular sea states.

For the PDB events, the area of the entrapped cavity showed a parabolic behaviour with the modified crest-front steepness. For the first water-on-deck events, the water-front velocity u along the deck indicated that the nonlinearities of the incoming waves play a role. The results showed a fair quantitative agreement with the best-fitting curve of the water-front velocities estimated along the ship centreline by Barcellona *et al.*

(2003) for three-dimensional water-on-deck experiments on blunt bows interacting with wave packets.

Finally, the main scenarios associated with water-shipping events have been identified and their existence in the W_w/W-steepness plane has been discussed. This was qualitative because of the limitations connected with the model assumptions. In particular, the present study is mainly relevant for stationary ships with blunt bow forms. The water-on-deck diagram in figure 20 corresponds to the first documented attempt, within this research field, to classify in a systematic way such phenomena and represents an important basis for further investigations of water-shipping events. The next step would be to generalize the results from the present investigation to a ship which is freely floating.

This work was partially supported by the Centre for Ships and Ocean Structures, NTNU, Trondheim, within the "Green Water Events and Related Structural Loads" project, and partially done within the framework of the "Programma Ricerche INSEAN 2005-2007" and "Programma di Ricerca sulla Sicurezza" funded by *Ministero Infrastrutture e Trasporti*.

REFERENCES

Barcellona, M., Landrini, M., Greco, M. & Faltinsen, O. M. 2003 An experimental investigation on bow water shipping. *J. Ship Res.* **47**, 327–346.

Birkhoff, G. 1962 Helmholtz and Taylor instabilities. *Proc. Symp. on Applied Mathematics*, vol. 55, pp. 55–76.

Campana, E. & Iafrati, A. 2001 Unsteady free surface waves by domain decomposition approach. *Proc. 16th Intl Workshop on Water Waves and Floating Bodies, Hiroshima, Japan*, pp. 1–4.

Colicchio, G., Greco, M. & Faltinsen, O. M. 2006 A bem-level set domain decomposition strategy for nonlinear and fragmented interfacial flows. *J. Numer. Meth. Engng* **67**, 1385–1419.

Colicchio, G., Landrini, M. & Chaplin, J. 2005 Level-set computations of free surface rotational flows. *Trans. ASME: J. Fluids Engng* **127**, 1111–1121.

Cooker, M. J. & Peregrine, D. H. 1992 Wave impact pressure and its effects upon bodies lying on the bed. *Coastal Engng* **18**, 205–229.

Faltinsen, O. M. 2005 *Hydrodynamics of High-speed Marine Vehicles*. Cambridge University Press.

Faltinsen, O. M., Landrini, M. & Greco, M. 2004 Slamming in marine applications. *J. Engng Maths* **48**, 448–475.

Faltinsen, O. M., Zhu, X. & Hu, C. 2005 Strongly nonlinear flows in seakeeping. Keynote lecture. *Proc. ICRMT'05, Ischia, Italy*, pp. 1–18.

Greco, M. 2001 A two-dimensional study of green-water loading. Dept Marine Hydrodynamics, NTNU, Trondheim, Norway (http://www.diva-portal.org/ntnu/theses/abstract.xsql?dbid=524).

Greco, M., Landrini, M. & Faltinsen, O. M. 2003 Local hydroelastic analysis on a VLFS with shallow draft. *Proc. Intl Conf. on Hydroelasticity in Marine Technology, Oxford, UK*.

Greco, M., Landrini, M. & Faltinsen, O. M. 2005 Shipping of water on a two-dimensional structure. *J. Fluid Mech.* **525**, 309–332.

Kjeldsen, S. P. & Myrhaug, D. 1979 Breaking waves in deep water and resulting wave forces. *Proc. 11th* Offshore Tech. Conf., Paper 3646.

Kleefsman, K. M. T., Fekken, G., Veldman, A. E. P., Bunnik, T. H. J., Buchner, B. & Iwanowski, B. 2002 Prediction of green water and wave loading using a Navier-Stokes based simulation tool. *Proc. 21st Intl Conf. on Offshore Mechanics and Artic Engineering, Norway*, Paper 28480, pp. 1–8.

Lugni, C., Brocchini, M., Bulgarelli, U. P., Faltinsen, O. M., Dolcini, A. & Palladino, F. 2005 An experimental investigation on the flip-through phenomenon. *20th Intl Workshop on Water Waves and Floating Bodies*, pp. 1–4.

MARINTEK 2000 *Review No. 1,* April. Merine Technology Centre, Trondheim, Norwey.

Nielsen, K. B. & Mayer, S. 2004 Numerical prediction of green water incidents. *Ocean Engng* **31**, 363–399.

Peregrine, D. H. 2003 Water-wave impact on walls. *Annu. Rev. Fluid Mech.* **35**, 23–43.

Quarteroni A. & Valli, A. 1999 *Domain Decomposition Methods for Partial Differential Equations.* Oxford Science Publications.

Sethian, J. A. 1999 *Level Set Methods and Fast Marching Methods: Evolving Interface in Computational Geometry, Fluid Mechanics, Computer Vsion and Materials Science.* Cambridge University Press.

Stoker, J. J. 1958 *Water Waves.* Wiley.

Walkden, M., Wood, D. J., Bruce, T. & Peregrine, D. H. 2001 Impulsive seaward loads induced by wave overtopping on caisson breakwaters. *Coastal Engng* **42**, 257–276.

Wehausen, J. V. & Laitone, E. V. 1960 *Handbuch der Physik* (ed. W. Fludge), vol. 9, pp. 446–778.

Wemmenhove, R., Loots, G. E., Luppes, R. & Veldman, A. E. P. 2005 Simulation of green water loading by a three-dimensional two-phase numerical model. *Proc. 20th Intl Workshop on Water Waves and Floating Bodies, Longyearbyen, Norway*, pp. 1–4.